Research Square

Preprints are preliminary reports that have not undergone peer review.
They should not be considered conclusive, used to inform clinical practice,
or referenced by the media as validated information.

Isogeometric thermal postbuckling analysis of geometrically imperfect sandwich plates

Vasudev Sengar
Sanjivani University
Gaurav Watts
Birla Institute of Technology and Science Pilani
Dhruv Deshwal
dhruvdeshwal17@gmail.com

Gramya Innovative Technologies

Research Article

Keywords: Auxetic core, Postbuckling, Sandwich Plate, NURBS, Isogeometric analysis, FGCNTRC plate

Posted Date: November 9th, 2026

DOI: https://doi.org/10.21203/rs.3.rs-11049313/v1

License: This work is licensed under a Creative Commons Attribution 4.0 International License.
Read Full License

Additional Declarations: No competing interests reported.

Isogeometric thermal postbuckling analysis of geometrically imperfect sandwich plates

Abstract:

This study uses isogeometric analysis (IGA) to explore how sandwich plates behave after buckling under thermal loads. The plates considered here have face sheets made of functionally graded carbon-nanotube reinforced composite (FG-CNTRC), whose material properties vary with temperature, while the core is a metallic auxetic structure with properties that can be tuned as needed. The governing equations are derived from Hamilton's principle, and NURBS basis functions are used to describe both the geometry and the field variables. Open uniform knot vectors are chosen to build the B-spline basis functions since they interpolate at the ends, which makes it straightforward to impose boundary conditions directly at the endpoints. To keep the computations efficient and speed up convergence, a k-refinement strategy is followed. The plate kinematics rest on a refined higher-order theory. When compared with results reported in the literature, the present predictions show good agreement. Finally, parametric studies are carried out to examine how the CNT distribution in the face sheets, the auxeticity of the core, and the plate aspect ratio affect the buckling response of these sandwich plates.

Keywords: Auxetic core; Postbuckling; Sandwich Plate; NURBS; Isogeometric analysis; FGCNTRC plate.

1. Introduction:

Sandwich structures are commonly used in civil, mechanical, aerospace, and marine structures [1]. A sandwich structure is made up of two face sheets separated by a lightweight core. It finds applications in various engineering fields due to its remarkable strength-to-weight ratio and exceptional energy absorption capability. Researchers have been recently working on using innovative core materials to further enhance the mechanical performance of sandwich structures. In 1987, polyurethane (PU) foam, which expands laterally when stretched, was initially identified by Lakes [1]. Subsequently, this unique phenomenon was later referred to as anti-rubber, auxetic, or dilatational materials by researchers [2]. The auxetic materials possess a negative Poisson's ratio and can expand laterally when subjected to tension [3,4,5]. Mir et al. [6] include a detailed discussion on different types of auxetic materials and their applications.

Honeycomb structures with re-entrant cell geometry have been found to perform better in mitigating blast loads and have the potential to replace existing materials used for protection in military vehicles and marine structures. The stability behaviour of sandwich structures with conventional honeycomb cores under mechanical or thermal loads has been investigated in the past by several researchers [7]. Thangaratnam et al. [7] reported the critical buckling temperatures of composite laminates under thermal loads using a finite element formulation. Na and Kim [8] used the three-dimensional finite element method to examine the thermal buckling and post-buckling behaviour of functionally graded materials (FGM) subjected to uniform or non-uniform temperature rise. The thermal post-buckling responses of FGM shell structures were reported by Trabelsi et al. [9]. Mehar et al. [10] analysed the buckling load parameters of the carbon nanotube (CNT) reinforced sandwich structure under the influence of uniform thermal loading. However, similar studies on sandwich structures with auxetic cores are scarce in the literature.

Harkati et al. [11] conducted a parametric investigation on a multi-reentrant honeycomb structure, examining its behaviour under variable stiffness and Poisson's ratio effects. Alipour and Shariyat [12] investigated the free vibration analysis of circular and annular sandwich plates with auxetic core and isotropic/orthotropic face sheets using a global layerwise theory. Sarafraz and Seidi [13] performed free vibration and buckling analyses on a sandwich plate with an auxetic honeycomb core and two laminated three-phase polymer/GNP/fibre face sheets by employing the sinusoidal shear deformation theory (SSDT) and the differential quadrature method (DQM). Li et al. [14] investigated the post-buckling behaviour of sandwich plates with FG auxetic 3D lattice cores. They compared the effect of thermal and mechanical loading on post-buckling behaviour using finite element (FE) modelling. Chen et al. [15] employed a 2-step perturbation technique in conjunction with Reddy's third-order shear deformation theory and explored the thermo-mechanical post-buckling behaviours of sandwich plates with

auxetic graphene-reinforced metal matrix composite (GRMMC) cores resting on elastic foundations. Quang et al. [16] presented a study on the non-linear static buckling behaviour of a magneto-electro-elastic sandwich plate, in which the sandwich plate comprised of an auxetic honeycomb core and two face sheets made up of magneto-electro-elastic material. They considered the plate's response under various loadings, including mechanical, thermal, electric, and magnetic, while accounting for the Pasternak-type elastic foundations. Existing studies on the thermal buckling and post-buckling behaviour of functionally graded carbon nanotube-reinforced composite (FG-CNTRC) plates [18]–[21] provide valuable insights into the buckling behaviour of varying plate configurations and materials, forming the basis for the present research. However, most of the previous works are based on temperature-independent properties. After an extensive literature survey, it may be concluded that similar studies on FGCNTRC structures with temperature-dependent properties are limited.

Isogeometric analysis (IGA) [22] is a numerical technique that uses NURBS-based approximation for geometrical and solution variables. IGA has shown promise in modelling complex structures with better accuracy and efficiency than traditional finite element analysis. The integration of HSDT and IGA presents a robust approach for comprehensively analysing composite sandwich plates. Few researchers have used an isogeometric formulation to investigate plate's buckling, post-buckling and post-buckled vibration behaviour [23]–[32]. Farzam and Hassani[33] used isogeometric analysis (IGA) with the modified couple stress theory to analyse the thermal and mechanical buckling behaviour of FG-CNTRC plates. Zhang et al. [34] presented IGA and Reddy's HSDT to study the influence of CNT orientation on the buckling behaviour of the FGCNTRC skew plate. Valizadeh et al.[35] carried out free, forced vibration, and buckling analysis of orthotropic plates using IGA based on first-order shear deformation theory. Le-Manh et al. [36] explored the post-buckling behaviour of composite plates using NURBS-based isogeometric analysis (IGA). It can be inferred from the detailed literature survey that there is a noticeable absence of existing literature that specifically investigates the thermal buckling and post-buckling behaviour of imperfect sandwich plates with an auxetic core.

In the present work, the isogeometric formulation, in conjunction with a refined higher-order theory, is employed to determine linear buckling and non-linear post-buckling behaviour with FGCNTRC face sheets and auxetic core under thermal loads. The governing equations are derived using the Hamilton principle, which includes temperature-dependent thermomechanical material properties and non-linear strain-displacement relations. The results obtained are compared to this model to ensure the accuracy and efficacy of the methodology adopted in the present work. Thereafter, new results on the influence of CNT distribution in the face sheets, different types of geometrical imperfections, parameters of the auxetic core, boundary conditions, and span-to-thickness ratios are presented for square sandwich plates.

1.1 Geometry and material properties:

Fig. 1. presents the geometrical parameters of the sandwich plate. The sandwich plate is composed of functionally graded carbon nanotube-reinforced composite (FG-CNTRC) materials with temperature-dependent properties of the constituent materials, as referenced in the source [37]. The thermomechanical properties of carbon nanotubes (CNTs) are calculated as a temperature function using a fourth-order interpolation approach:

$$P = P_0 + P_1\left(\frac{T}{T_0}\right) + P_2\left(\frac{T}{T_0}\right)^2 + P_3\left(\frac{T}{T_0}\right)^3 + P_4\left(\frac{T}{T_0}\right)^4 \quad (1)$$

The face sheets are nanocomposites of CNTs and polymethyl methacrylate (PMMA) matrix (E_m = 2.5 GPa, ν_m = 0.3, ρ_m = 1150 kg/m^3). The unique coefficients P_i are given in Table 1 for each thermomechanical property. The distribution of CNTs in the face sheets influences the effective material properties. The three types of CNT distributions through the face sheets' thickness, UD, FGX and FGO, are shown in Fig. 2. The functions corresponding to the graded distributions of CNTs are given in Table 2a. The total volume fraction of CNTs in all three cases is assumed to be the same.

Table 1. Coefficients P_i associated to fourth-order interpolation for various thermomechanical properties [37]

P	P_0	P_1	P_2	P_3	P_4
E_{11}[TPa]	+6.56537	-1.76156	+1.13347	-0.32260	+0.03193

E_{22}[TPa]	+8.22710	-2.19725	+1.41176	-0.40125	+0.03964
G_{12}[TPa]	+1.10442	+1.88427	-1.47623	+0.49029	-0.05829
$\alpha_{11}[10^{-6}/^{\circ}C]$	-1.12800	+6.88290	-2.60621	+0.31023	-0.00054
$\alpha_{22}[10^{-6}/^{\circ}C]$	+5.43593	-0.29201	+0.02268	+0.00182	-0.00023
ν_{12}	+0.17500	0	0	0	

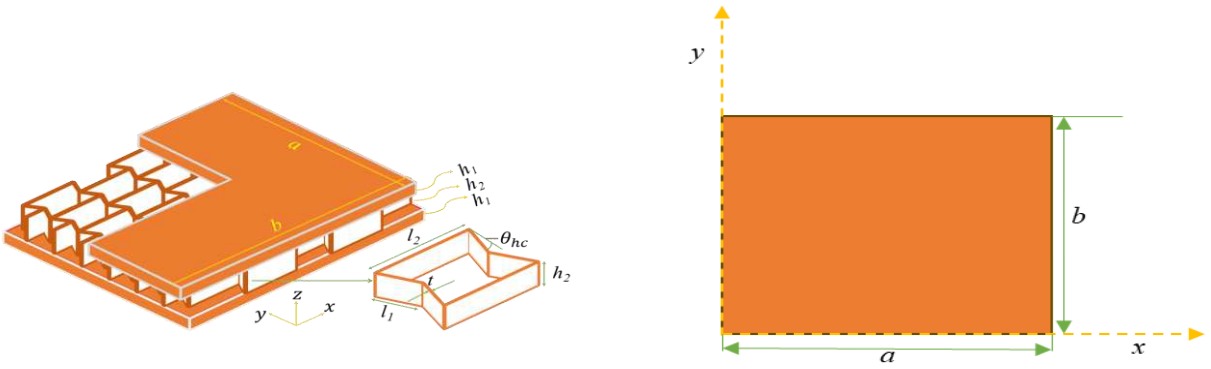
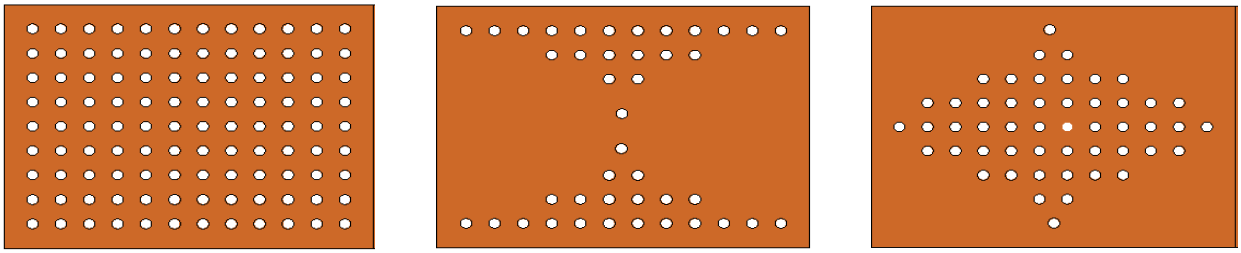


Fig. 1. Geometrical parameters for the sandwich plate



(a) UD (b) FGX (c) FGO

Fig. 2. Different CNT distributions in the top and bottom face sheets.

Table 2. Volume fraction function of CNTs for different distributions

CNTs distribution type	UD	FGX	FGO
Volume Fraction of CNTs in face sheets	V_{CN}^{*}	$\frac{4}{h_t - h_b}\left(\left\|\frac{h_t + h_b}{2} - z\right\|\right) V_{CN}^{*}$	$\frac{4}{h_t - h_b}\left(\frac{h_t - h_b}{2} - \left\|\frac{h_t + h_b}{2} - z\right\|\right) V_{CN}^{*}$

In Table 2, h_t and h_b are the z coordinates of the end positions of face sheets. The extended rule of mixtures with efficiency parameters is used to evaluate the effective material properties of the face sheets, which are given by:

$$E_{11} = \eta_1 V_{CN} E_{11}^{CN} + V_m E_m$$

$$\frac{\eta_2}{E_{22}} = \frac{V_{CN}}{E_{22}^{CN}} + \frac{V_m}{E_m}$$

$$\frac{\eta_3}{G_{12}} = \frac{V_{CN}}{G_{12}^{CN}} + \frac{V_m}{G_m}$$

$$\nu_{12} = V_{CN}^{*} \nu_{12}^{CN} + V_m \nu_m \quad (2)$$

E_{11}^{CN}, E_{22}^{CN}, G_{12}^{CN} and ν_{12}^{CN} are in-plane Young's moduli, shear moduli and Poisson's ratio of CNTs, respectively. E_m, G_m and ν_m are the Young's moduli, shear moduli and Poisson's ratio for the PMMA matrix. V_{CN} and V_m are

the volume fractions of CNT and the matrix, respectively. The material properties of the resultant FGCNTRCs are assumed to be scale-dependent [38]. The scale dependency of material properties is incorporated by determining the efficiency parameters. The efficiency parameters (η_1, η_2, η_3) considered in the present investigation are given in Table 2a.

Table 2a. Efficiency parameters for the FGCNTRC[39]

Volume Fraction (V_{CN}^{*})	Efficiency Parameters
0.12	$\eta_1 = 0.137, \eta_2 = 1.022, \eta_3 = 0.7\eta_2$
0.17	$\eta_1 = 0.142, \eta_2 = 1.626, \eta_3 = 0.7\eta_2$
0.28	$\eta_1 = 0.141, \eta_2 = 1.585, \eta_3 = 0.7\eta_2$

The present study considers an auxetic core with a negative Poisson ratio. $E_{11}^{(c)}$, $E_{22}^{(c)}$, $G_{12,}^{C}G_{23}^{(c)}$, $G_{13}^{(c)}$ and $\nu_{12}^{(C)}$ $\nu_{21}^{(c)}$ are Young's moduli shear moduli and Poisson's ratio of the auxetic core. $\rho^{(c)}$ is the density of the honeycomb material, i.e., aluminium. The honeycomb plate core gives the material properties (E = 69 GPa, ν = 0.3, G = 27 GPa and ρ = 2700 kg/m^3) [40].

$$E_{11}^{(c)} = E\left(\frac{t}{l_1}\right)^3 \frac{\left(\frac{l_2}{l_1} - \sin\theta_{hc}\right)}{\cos\theta_{hc}\left[1 + \left(\tan^2\theta_{hc} + \frac{l_2}{l_1}\sec^2\theta_{hc}\right)\left(\frac{t}{l_1}\right)^2\right]}$$

$$E_{22}^{(c)} = E\left(\frac{t}{l_1}\right)^3 \frac{1}{\cos\theta_{hc}\left(\frac{l_2}{l_1} - \sin\theta_{hc}\right)\left(\tan^2\theta_{hc} + \left(\frac{t}{l_1}\right)^2\right)}$$

$$G_{12}^{(c)} = G\left(\frac{t}{l_1}\right)^3 \frac{1}{\left(\frac{l_2}{l_1}\right)\left(1 + 2\frac{l_2}{l_1}\right)\cos\theta_{hc}}$$

$$G_{23}^{(c)} = G\left(\frac{t}{l_1}\right)\frac{\cos\theta_{hc}}{\left(\frac{l_2}{l_1} - \sin\theta_{hc}\right)} \tag{3}$$

$$G_{13}^{(c)} = G\frac{\left(\frac{t}{l_1}\right)}{2\cos\theta_{hc}}\left[\frac{\left(\frac{h_2}{l_1} - \sin\theta_{hc}\right)}{\left(1 + 2\frac{l_2}{l_1}\right)} + \frac{\left(\frac{l_2}{l_1} + 2\sin^2\theta_{hc}\right)}{2\left(\frac{h_2}{l_1} - \sin\theta_{hc}\right)}\right]$$

$$v_{12}^{(c)} = -\frac{\sin\theta_{hc}\left(1 - \left(\frac{t}{l_1}\right)^2\right)\left(\frac{h_2}{l_1} - \sin\theta_{hc}\right)}{\cos^2\theta_{hc}\left[1 + \left(\tan^2\theta_{he} + \frac{l_2}{l_1}\sec^2\theta_{hc}\right)\left(\frac{t}{l_1}\right)^2\right]}$$

$$v_{21}^{(c)} = -\frac{\sin\theta_{hc}\left(1 - \left(\frac{t}{l_1}\right)^2\right)}{\left(\tan^2\theta_{hc} + \left(\frac{t}{l_1}\right)^2\right)\left(\frac{l_2}{l_1} - \sin\theta_{hc}\right)}$$

$$\rho^{(c)} = \rho\frac{\left(\frac{t}{t_1}\right)\left(\frac{t_2}{t_1} + 2\right)}{2\cos\theta_{hc}\left(\frac{t_2}{l_1} - \sin\theta_{hc}\right)}$$

Where l_1 is the length of the inclined cell rib, l_2 is the length of the vertical cell rib, t is the rib thickness, and θ_{hc} is the inclined cell angle. as shown in Fig. 1. Additionally, h_2 refers to the thickness of the core, and h_1 represents the face sheet thickness of the top layer, which is equal to the thickness of the bottom layer.

2 Mathematical Formulation:

2.1 Isogeometric Analysis (IGA):

IGA, an engineering analysis methodology based on using the exact representation of geometry, was proposed by Hughes et al. [22]. In IGA, the geometric and field variables are approximated using non-uniform rational B-Spline (NURBS) basis functions. The B-Spline basis functions are derived through the use of the Cox-de Boor recursion formula, which is presented below:

$$N_{i,0}(\xi) = \begin{cases} 1 & \xi_i \le \xi < \xi_{i+1} \\ 0 & otherwise \end{cases} \tag{4}$$

$$N_{i,p}(\xi) = \frac{\xi - \xi_i}{\xi_{i+p} - \xi_i} N_{i,p-1}(\xi) + \frac{\xi_{i+p+1} - \xi}{\xi_{i+p+1} - \xi_{i+1}} N_{i+1,p-1}(\xi) \tag{5}$$

Here ξ is the knot value in the knot vector $\Xi = \{\xi_1, \xi_2, \dots, \xi_{n+p+1}\}$ p is the degree of the B-Spline curve, and n is the number of control points in the physical space.

A two-dimensional NURBS basis function is defined as follows:

$$R_{i,j}^{p,q} = \frac{N_{i,p}(\xi) M_{j,q}(\eta) w_{i,j}}{\sum_{i=1}^{n} \sum_{j=1}^{m} N_{i,p}(\xi) N_{j,q}(\eta) w_{i,j}} \tag{6}$$

$N_{i,p}$ and $M_{j,q}$ are the B-Spline basis functions with orders p, q respectively in two different directions defined by the knot vectors, $\Xi = \{\xi_1, \xi_2, \dots, \xi_{n+p+1}\}$, $\Omega = \{\eta_1, \eta_2, \dots, \eta_{n+p+1}\}$ in the parameter space, n, m is the number of control points in the respective directions.

The coordinates and the solution variables are approximated as a linear combination of basis functions, and the values of the variable at control points are as follows:

$$S(\xi, \eta) = \sum_{i=1}^{n} \sum_{j=1}^{m} R_{i,j}^{p,q} P_{i,j} \tag{7}$$

Where $P_{i,j}$ signifies the subsequent values at the control points.

2.2 Governing Equations: The plate's mid-plane is discretised using control points. The displacement field is modelled using a refined higher-order model [41]

$$u(x, y, z) = u_0(x, y) - z \frac{\partial w_0(x, y)}{\partial x} + f(z)\theta_x(x, y) \tag{8}$$

$$v(x, y, z) = v_0(x, y) - z \frac{\partial w_0(x, y)}{\partial y} + f(z)\theta_y(x, y) \tag{9}$$

$$w(x, y, z) = w_0(x, y) \tag{10}$$

Where $f(z) = \left(z e^{1 - \frac{4z^2}{h^2}} + z \right)$ allows the sandwich laminate to satisfy zero transverse shear stress criteria at the top and bottom positions. u_0, v_0 are in-plane displacements and w_0 is the transverse displacement at a point on the middle plane. θ_y and θ_x are the normal to the mid-plane rotations about the x and y-axis, respectively.

The approximations of the displacements are obtained by using NURBS basis functions in the following manner:

$$q = \begin{Bmatrix} u_0 \\ v_0 \\ w_0 \\ \theta_x \\ \theta_y \end{Bmatrix} = \sum_{i=1}^{n \times m} \begin{bmatrix} \varphi_i & 0 & 0 & 0 & 0 \\ 0 & \varphi_i & 0 & 0 & 0 \\ 0 & 0 & \varphi_i & 0 & 0 \\ 0 & 0 & 0 & \varphi_i & 0 \\ 0 & 0 & 0 & 0 & \varphi_i \end{bmatrix} \begin{Bmatrix} u_{0i} \\ v_{0i} \\ w_{0i} \\ \theta_{xi} \\ \theta_{yi} \end{Bmatrix} = \sum_{i=1}^{n \times m} \varphi_i \mathrm{q_i} \tag{11}$$

where φ_i is the NURBS-based approximation function and $\left(u_{0i}, v_{oi}, w_{0i}, \theta_{xi}, \theta_{yi}\right)^T$ are the degrees of freedom of control point P_i.

The strain displacement relations are as follows:

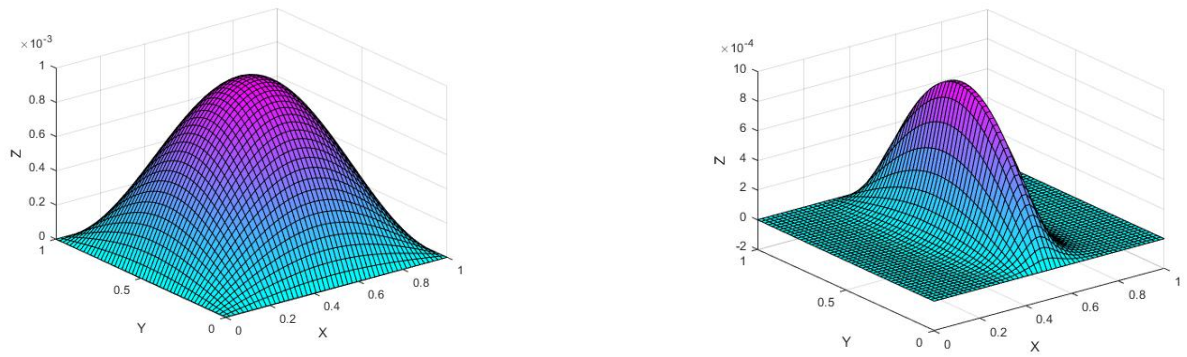
$$\begin{Bmatrix}\varepsilon_{xx}\\ \varepsilon_{yy}\\ \gamma_{xy}\end{Bmatrix}=\begin{Bmatrix}\frac{\partial u_0}{\partial x}\\ \frac{\partial v_0}{\partial y}\\ \frac{\partial u_0}{\partial y}+\frac{\partial v_0}{\partial x}\end{Bmatrix}-z\begin{Bmatrix}\frac{\partial^2 w_0}{\partial x^2}\\ \frac{\partial^2 w_0}{\partial y^2}\\ 2\frac{\partial^2 w_0}{\partial x\partial y}\end{Bmatrix}+f(z)\begin{Bmatrix}\frac{\partial \theta_x}{\partial x}\\ \frac{\partial \theta_y}{\partial y}\\ \frac{\partial \theta_x}{\partial y}+\frac{\partial \theta_y}{\partial x}\end{Bmatrix}+\frac{1}{2}\begin{Bmatrix}\left(\frac{\partial w_0}{\partial x}\right)^2\\ \left(\frac{\partial w_0}{\partial y}\right)^2\\ 2\frac{\partial w_0}{\partial x}\frac{\partial w_0}{\partial y}\end{Bmatrix} \tag{12a}$$

$$\begin{Bmatrix}\gamma_{xz}\\ \gamma_{yz}\end{Bmatrix}=\frac{\partial f(z)}{\partial z}\begin{Bmatrix}\theta_x\\ \theta_y\end{Bmatrix} \tag{12b}$$

An imperfection function combines trigonometric and hyperbolic functions and was introduced previously by Kitipornchai et al. [42]. The amplitude and localisation of a geometric imperfection can be modified through the parameters in the imperfection function below:

$$w^*=\eta h\, sec\, h\left[\delta_1\left(\frac{x}{a}-\psi_1\right)\right]cos\left[\mu_1\pi\left(\frac{x}{a}-\psi_1\right)\right]\times sec\, h\left[\delta_2\left(\frac{y}{b}-\psi_2\right)\right]cos\left[\mu_2\pi\left(\frac{y}{b}-\psi_2\right)\right] \tag{13}$$

In the given context, the symbol μ denotes the amplitude of imperfection, which exhibits values ranging from 0 to 1. The constants δ_1 and δ_2 indicates the localised degree of the imperfection, which possesses symmetry concerning $\frac{x}{a}=\psi_1$ and $\frac{y}{b}=\psi_2$ respectively. Additionally, μ_1 and μ_2 represent the half wave numbers of the imperfection along the x and y axes, correspondingly. h is the thickness of the plate.



(a) Sine type (b) L_2 type

$\delta_1=\delta_2=0,\mu_1=\mu_2=1,\psi_1=\psi_2=0.5$ $\delta_1=15,\delta_2=0,\mu_1=2,\mu_2=1,\psi_1=0.5,\psi_2=0.5$

Fig 3. Types of geometric imperfection modes[42]

The strains due to initial imperfection at the mid-surface can be written as

$$\varepsilon_x^*=\frac{1}{2}\left(w_{,x}^*\right)^2;\quad \varepsilon_y^*=\frac{1}{2}\left(w_{,y}^*\right)^2;\quad \gamma_{xy}^*=w_{,x}^*w_{,y}^*;\quad \gamma_{xz}^*=w_{,x}^*\,;\,\gamma_{yz}^*=w_{,y}^* \tag{14}$$

The net strains, after including initial imperfections, can be rewritten as:

$$\varepsilon_1=\varepsilon_m-z\varepsilon_h+f(z)\varepsilon_b+\varepsilon_{nl}+\varepsilon_I \tag{15a}$$

$$\text{Where } \varepsilon_m=\sum_{i=1}^{ncp}\begin{bmatrix}\varphi_{i,x} & 0 & 0 & 0 & 0\\ 0 & \varphi_{i,y} & 0 & 0 & 0\\ \varphi_{i,y} & \varphi_{i,x} & 0 & 0 & 0\end{bmatrix}\begin{bmatrix}u_{0i}\\ v_{oi}\\ w_{0i}\\ \theta_{xi}\\ \theta_{yi}\end{bmatrix}=\boldsymbol{B_m q} \tag{15b}$$

$$\varepsilon_h = \sum_{i=1}^{ncp} \begin{bmatrix} 0 & 0 & \varphi_{i,x\,x} & 0 & 0 \\ 0 & 0 & \varphi_{i,y\,y} & 0 & 0 \\ 0 & 0 & 2\varphi_{i,x\,y} & 0 & 0 \end{bmatrix} \begin{bmatrix} u_{0i} \\ v_{oi} \\ w_{0i} \\ \theta_{xi} \\ \theta_{yi} \end{bmatrix} = \boldsymbol{B_h q} \tag{15c}$$

$$\varepsilon_b = \sum_{i=1}^{ncp} \begin{bmatrix} 0 & 0 & 0 & \varphi_{i,x} & 0 \\ 0 & 0 & 0 & 0 & \varphi_{i,y} \\ 0 & 0 & 0 & \varphi_{i,y} & \varphi_{i,x} \end{bmatrix} \begin{bmatrix} u_{0i} \\ v_{oi} \\ w_{0i} \\ \theta_{xi} \\ \theta_{yi} \end{bmatrix} = \boldsymbol{B_b q} \tag{15d}$$

$$\varepsilon_I = \begin{Bmatrix} \frac{\partial w_0}{\partial x}\frac{\partial w^*}{\partial x} \\ \frac{\partial w_0}{\partial y}\frac{\partial w^*}{\partial y} \\ \frac{\partial w_0}{\partial x}\frac{\partial w^*}{\partial y} + \frac{\partial w_0}{\partial y}\frac{\partial w^*}{\partial x} \end{Bmatrix} = \sum_{i=1}^{ncp} \begin{bmatrix} w_x^* & 0 \\ 0 & w_y^* \\ w_y^* & w_x^* \end{bmatrix} \begin{bmatrix} 0 & 0 & \varphi_{i,x} & 0 & 0 \\ 0 & 0 & \varphi_{i,y} & 0 & 0 \end{bmatrix} = \boldsymbol{B_I q} \tag{15e}$$

$$\varepsilon_{nl} = \sum_{i=1}^{ncp} \frac{1}{2} \begin{bmatrix} w_{0,x} & 0 \\ 0 & w_{0,y} \\ w_{0,y} & w_{0,x} \end{bmatrix} \begin{bmatrix} 0 & 0 & \varphi_{i,x} & 0 & 0 \\ 0 & 0 & \varphi_{i,y} & 0 & 0 \end{bmatrix} \begin{bmatrix} u_{0i} \\ v_{oi} \\ w_{0i} \\ \theta_{xi} \\ \theta_{yi} \end{bmatrix} = \boldsymbol{B_{nl} q} \tag{15f}$$

$$\varepsilon_2 = \sum_{i=1}^{ncp} \left[\frac{\partial f(z)}{\partial z}\right] \begin{bmatrix} 0 & 0 & 0 & \varphi_i & 0 \\ 0 & 0 & 0 & 0 & \varphi_i \end{bmatrix} \begin{bmatrix} u_{0i} \\ v_{oi} \\ w_{0i} \\ \theta_{xi} \\ \theta_{yi} \end{bmatrix} = \boldsymbol{B_\gamma q} \tag{15g}$$

In relation to the thermal effect, the thermal strain can be expressed as follows:

$$\boldsymbol{\varepsilon}^{\text{th}} = \alpha \Delta T [1 \quad 1 \quad 0]^T \tag{16}$$

where $\Delta T = T - T_i$ let T_i represent the original temperature, and T denote the present temperature. In the context of plate theories, the transverse normal stress is assumed to be negligible. Therefore, the simplified constitutive relation for the plate can be expressed as follows.

$$\begin{Bmatrix} \boldsymbol{\sigma} \\ \boldsymbol{\tau} \end{Bmatrix} = \begin{bmatrix} \boldsymbol{Q} & \boldsymbol{0} \\ \boldsymbol{0} & \boldsymbol{P} \end{bmatrix} \begin{Bmatrix} \varepsilon_1 - \varepsilon^{\text{th}} \\ \varepsilon_2 \end{Bmatrix} \tag{17}$$

The stress-strain relations for k^{th} lamina can be written as:

$$\begin{bmatrix} \sigma_{xx} \\ \sigma_{yy} \\ \tau_{xy} \end{bmatrix}^k = \begin{bmatrix} Q_{11}^k & Q_{12}^k & 0 \\ Q_{21}^k & Q_{22}^k & 0 \\ 0 & 0 & Q_{33}^k \end{bmatrix} \begin{bmatrix} \varepsilon_{xx} \\ \varepsilon_{yy} \\ \gamma_{xy} \end{bmatrix}^k \text{ and } \begin{bmatrix} \tau_{yz} \\ \tau_{xz} \end{bmatrix}^k = \begin{bmatrix} P_{11}^k & 0 \\ 0 & P_{22}^k \end{bmatrix} \begin{bmatrix} \gamma_{yz} \\ \gamma_{xz} \end{bmatrix}^k \tag{18}$$

Where

$$Q_{11} = \frac{E_1}{1-\nu_{12}\nu_{21}}; Q_{22} = \frac{E_2}{1-\nu_{12}\nu_{21}}; Q_{12} = Q_{21} = \frac{E_2\nu_{12}}{1-\nu_{12}\nu_{21}}; Q_{33} = G_{12}; P_{11} = G_{23}; P_{22} = G_{12}$$

The in-plane forces, moments, higher-order forces and shear forces are expressed as

$$\begin{Bmatrix} \boldsymbol{N} \\ \boldsymbol{M} \\ \boldsymbol{P} \\ \boldsymbol{R} \end{Bmatrix} = \begin{bmatrix} \boldsymbol{A} & \boldsymbol{B} & \boldsymbol{E} & \boldsymbol{0} \\ \boldsymbol{B} & \boldsymbol{D} & \boldsymbol{F} & \boldsymbol{0} \\ \boldsymbol{E} & \boldsymbol{F} & \boldsymbol{H} & \boldsymbol{0} \\ \boldsymbol{0} & \boldsymbol{0} & \boldsymbol{0} & \boldsymbol{D}^{s} \end{bmatrix} \begin{Bmatrix} \varepsilon_m \\ \varepsilon_h \\ \varepsilon_b \\ \varepsilon_\gamma \end{Bmatrix} - \begin{Bmatrix} \boldsymbol{N}^{\text{th}} \\ \boldsymbol{M}^{\text{th}} \\ \boldsymbol{P}^{\text{th}} \\ 0 \end{Bmatrix} = \widehat{\boldsymbol{D}}_u \hat{\varepsilon} - \hat{\sigma}_0 \tag{19}$$

$$\begin{Bmatrix} \boldsymbol{N} \\ \boldsymbol{M} \\ \boldsymbol{P} \end{Bmatrix} = \int_{-\frac{h}{2}}^{\frac{h}{2}} \boldsymbol{\sigma} \begin{Bmatrix} 1 \\ z \\ f(z) \end{Bmatrix} dz \text{ and } \boldsymbol{R} = \int_{-\frac{h}{2}}^{\frac{h}{2}} f'(z)\tau dz \tag{20}$$

$$\left(A_{ij}, B_{ij}, D_{ij}, E_{ij}, F_{ij}, H_{ij}\right) = \int_{-h/2}^{h/2} Q_{ij}(1, z, z^2, f(z), zf(z), f^2(z))dz$$

,

$$D^s_{\alpha\beta} = \int_{-h/2}^{h/2} (f'(z))^2 P_{\alpha\beta} dz, (i, j, k = 1,2,3; \alpha, \beta = 1,2)$$

The thermal stress resultants are dependent on the incremental temperature.

$$\{\boldsymbol{N}^{\text{th}} \quad \boldsymbol{M}^{\text{th}} \quad \boldsymbol{P}^{\text{th}}\} = \int_{-\frac{h}{2}}^{\frac{h}{2}} \boldsymbol{Q_{ij}} \begin{Bmatrix} \alpha \\ \alpha \\ 0 \end{Bmatrix} \{1 \quad z \quad f(z)\} \Delta T dz \tag{21}$$

The plate's total energy variation can be calculated using the principle of virtual displacement.

$$\delta \Pi = \delta U_\varepsilon - \delta V = \int_\Omega \delta \hat{\varepsilon}^T \hat{\sigma} d\Omega - \int_\Omega \delta u^T f_z d\Omega = 0 \tag{22}$$

From equations (11) and (12), generalised strains can be rewritten in matrix form as

$$\hat{\boldsymbol{\varepsilon}} = \left(\boldsymbol{B_L} + \frac{1}{2}\boldsymbol{B_{NL}}\right)\boldsymbol{q_i} \tag{23}$$

$$\boldsymbol{B}^i_L = \left[(\boldsymbol{B}^i_m)^T \left(\boldsymbol{B}^i_b\right)^T \left(\boldsymbol{B}^i_h\right)^T \left(\boldsymbol{B}^i_{\boldsymbol{\gamma}}\right)^T\right]^T \tag{24}$$

Variation of the strain is defined as

$$\delta\hat{\boldsymbol{\varepsilon}} = (\boldsymbol{B_L} + \boldsymbol{B_{NL}})\delta\boldsymbol{q_i} \tag{25}$$

Substituting Eqs. (20) and (23) into Eq. (22), the governing equation can be written in the following matrix for

$$(\boldsymbol{K}_L + \boldsymbol{K}_{NL} - \boldsymbol{K}_G)\boldsymbol{q_i} = \boldsymbol{F} \tag{26}$$

The linear stiffness matrix is denoted as K_L, while the non-linear stiffness matrix is denoted as K_{NL}. Additionally, K_G represents the initial stress stiffness matrix resulting from the initial compressive force caused by temperature. The load vector, designated as F, depends on mechanical and thermal loads.

After determining the critical buckling parameter via the resolution of the non-linear eigenvalue problem described in Eq. (26), the post-buckling equilibrium path is obtained using the iterative and incremental procedure via the Newton–Raphson method. This iterative method keeps going until the convergence of the thermal buckling temperature is achieved.

2.3 Boundary conditions: The boundary conditions considered in the present investigation are given by:

(A) Simply supported **:**(SSSS) : $\begin{cases} u_0 = v_0 = w_0 = \theta_y = 0 \text{ on } x = 0, a \\ u_0 = v_0 = w_0 = \theta_x = 0 \text{ on } y = 0, b \end{cases}$

$\text{S}^1\text{S}^1\text{S}^1\text{S}^1$: $\begin{cases} v_0 = w_0 = \theta_y = 0 \text{ on } x = 0, a \\ u_0 = w_0 = \theta_x = 0 \text{ on } y = 0, b \end{cases}$

(B) Clamped support**: (**CCCC)**:** $\begin{cases} u_0 = v_0 = w_0 = \theta_x = \theta_y = 0 \\ w_{0,x} = w_{0,y} = 0 \end{cases}$ All edges

In the present article SSSS, boundary conditions are used for all the cases unless a particular case is specified.

3 Results and discussions:

3.1 Linear thermal buckling:

A MATLAB code has been developed for linear buckling and non-linear post-buckling analysis of square sandwich plates under thermal loading conditions. To ascertain the accuracy of the code, a validation study is conducted first.

Table 3. Comparison study of critical buckling temperature (ΔT_{cr} in Kelvin) for isotropic square plates under uniform temperature distribution for simply supported (SSSS) and clamped (CCCC) boundary conditions (a/h = 100 $\alpha = 2\times10^{-6}$)

a/h	p	nk	NCP	SSSS	CCCC
100	3	3	7× 7	63.36	168.94
		5	9 × 9	63.23	167.78
		7	11× 11	63.23	167.54
		9	13× 13	63.23	167.51
		11	15× 15	63.23	167.50
		13	17 × 17	63.23	167.49
		15	19 × 19	63.23	167.49
		Trabelsi et al.[43]		63.32	168.17
		Thangaratnam et al.[7]		63.33	167.70

Table 3 presents the convergence and solutions of the critical buckling temperature (ΔT_{cr} in K) for the isotropic square plates under uniform temperature distribution and for two types of boundary conditions. It includes the results obtained from the present formulation as well as analytical solutions reported by Thangaratnam et al. [7] and finite element solutions by Trabelsi et al. [43]. The present results are found to be in good agreement with existing solutions in the literature. The solution converges for 13-knot insertions; thus, the same number of knot insertions are used for subsequent results.

Table 4. Convergence of critical buckling temperature parameter, (T_{cr} in K) for SSSS FGCNTRC square plates based on a temperature-dependent analysis

a/h	nk	NCP	0.12		0.17		0.28	
			UD	FGX	UD	FGX	UD	FGX
10	9	13× 13	389.41	403.18	400.65	417.68	393.37	409.23
	11	15× 15	389.40	403.18	400.65	417.67	393.36	409.23
	13	17 × 17	389.40	403.18	400.65	417.67	393.36	409.23
	15	19 × 19	389.40	403.18	400.65	417.67	393.36	409.23
	Shen and Zhang [44]		388.19	403.91	399.44	419.09	391.62	410.58
	Kiani[45]		387.63	402.25	399.03	419.13	390.81	415.79

Non-dimensional critical buckling temperature parameter (T_{cr}) for SSSS FGCNTRC square plates subjected to thermal load are tabulated in Table 4. The values obtained are compared to the results of Shen and Zhang [44] and Kiani [45], and are matching well. It is observed from Table 4 that the non-dimensional critical buckling temperature parameter increases with the volume fraction of CNT.

Table 5.Critical temperature($\Delta T_{cr}\ in\ K$) of the isotropic imperfect ceramic plate for different imperfection modes under uniform temperature rise ($\alpha=7.4\times10^{-6}$, E=380 GPa and a/h = 100, $S^1S^1S^1S^1$) with sinusoidal imperfections.

μ	Imperfection Mode	
	Present	Cetkovic – LWT [46]
0	17.0894	17.277
0.1	17.2324	17.314

0.2	17.6600	17.654
0.3	18.3690	18.294
0.4	19.3534	19.233
0.5	20.6051	20.469
0.6	22.1127	22.000
0.7	23.8621	23.822
0.8	25.8357	25.930
0.9	28.0122	28.321
1	30.3663	30.987

The accuracy of the present refined higher-order theory [41] in modelling imperfect plates is confirmed by a comparison of the present results with those by Cetkovic[46] based on layerwise theory in Table 5. The results indicate that critical temperature increases steadily with the increase of imperfection amplitude μ from 0 to 1.

Table 6. Critical buckling temperature (ΔT_{cr} in K) of the SSSS square sandwich plate with auxetic core for two different imperfection modes under a uniform temperature rise ($\alpha=10^{-6}$, $l_2/l_1 = 2$, $t/l_1 = 0.1$, $h_2/h=0.5$ and a/h = 100, $\theta_{hc} = 30°$)

μ	Imperfection mode					
	10		20		100	
	S	L_2	S	L_2	S	L_2
0	218.8950	218.8950	81.4072	81.4072	3.8868	3.8868
0.1	226.7205	219.8575	83.6416	81.6942	3.9837	3.8994
0.2	249.7625	222.2592	90.2869	82.5025	4.2731	3.9367
0.3	286.6976	225.2103	101.1649	83.7012	4.7514	3.9965
0.4	335.1496	228.1453	115.9572	85.1378	5.4117	4.0758
0.5	375.2046	230.8894	134.1621	86.6851	6.2426	4.1712
0.6	375.9160	233.4550	155.0191	88.2589	7.2256	4.2789
0.7	376.7536	235.9023	174.0783	89.8138	8.3328	4.3954
0.8	377.7159	238.2882	190.4021	91.3311	9.1583	4.5177
0.9	378.8012	240.6545	208.1551	92.8075	10.0348	4.6431
1	380.0075	243.0293	212.9974	94.2469	10.9912	4.7698

Table 6 shows the influence of two imperfection modes with different width-to-thickness ratios on critical buckling temperature of SSSS square sandwich plate with an auxetic core. As the imperfection amplitude increases and the width-to-thickness ratio decreases, the critical buckling temperature for the square sandwich plate increases. The results are expected since, with increasing the thickness, the flexural rigidity of the plate increases.

Table 7. Influence of type of CNT distribution in face sheets on critical buckling temperature (ΔT_{cr} in K) for the square sandwich plate for uniform temperature rise ($\alpha =10^{-6}$, $l_2/l_1 = 2$, $t/l_1 = 0.1$, $h_2/h = 0.5$ and a/h = 100)

V_{CN}^*	SSSS			CCCC		
	UD	FGX	FGO	UD	FGX	FGO
0.12	3.6874	3.8596	3.7285	13.9563	14.6206	14.0903
0.17	3.8890	4.1413	3.9826	14.5504	15.5048	14.8737
0.28	4.3479	4.8675	4.6132	16.1929	18.1156	17.1520

The influence of the type of carbon nanotube (CNT) distribution in the face sheets on the thermal buckling load of a sandwich plate with an auxetic core is included in Table 7. The buckling loads are presented for different carbon nanotube (CNT) distributions, volume fractions, and boundary conditions. The findings suggest that augmenting the concentration of carbon nanotubes (CNTs) in the face sheets leads to an increment in the critical buckling loads for a particular CNT distribution pattern. This phenomenon can be attributed to the change in the effective elasticity modulus and the overall stiffness of the plate. The buckling loads exhibit the highest values for the FGX distribution, followed by FGO, and the lowest for the UD distribution, given a specific boundary condition and CNT volume percentage.

Table 8. Influence of cell angle on critical buckling temperature parameter(ΔT_{cr} in K)) for a square sandwich plate (h_2/h =0.5 and a/h = 100, $\alpha = 10^{-6}$) for uniform temperature rise.

θ_{hc}	l_1/l_2							
	SSSS				CCCC			
	1.5	2	2.5	3	1.5	2	2.5	3
-30°	3.9089	3.9074	3.9064	3.9057	14.6565	14.6539	14.6527	14.6523
-15°	3.9004	3.8989	3.8980	3.8975	14.5774	14.5787	14.5801	14.5814
15°	3.8877	3.8841	3.8826	3.8820	14.6065	14.5891	14.5820	14.5790
30°	3.8904	3.8868	3.8858	3.8858	14.7193	14.6793	14.6616	14.6528

Table 9. Influence of core to plate thickness ratio on critical temperature parameter (ΔT_{cr} in K) for the square sandwich plate for uniform temperature rise ($t/l_1 = 0.1$, and a/h = 100, $l_1/l_2 = 2$, $\alpha = 10^{-6}$)

θ_{hc}	SSSS			CCCC		
	$h_2/h = 0.2$	$h_2/h = 0.5$	$h_2/h = 0.8$	$h_2/h = 0.2$	$h_2/h = 0.5$	$h_2/h = 0.8$
-30	2.7485	3.9074	5.6879	10.2791	14.6539	21.2134
-15	2.7461	3.8989	5.6429	10.2448	14.5787	21.0916
15	2.7464	3.8841	5.4630	10.2537	14.5891	20.9787
30	2.7499	3.8868	5.4231	10.3046	14.6793	20.9661

The influence of cell angle (θ_{hc}) of the auxetic core on the critical buckling temperature of the sandwich plate is studied in Table 8. It can be inferred that the change in cell angle and rib thickness ratio (l_1/l_2) has minimal effect on the results. Table 9 includes the results for three distinct ratios of the core layer thickness (h_2/h) to that of the sandwich laminate (h). The thickness of the top and bottom face sheets of the sandwich laminate is the same. The sandwich plate's buckling load increases when the ratio of h_2 to h increases. This can be attributed to the fact that the auxetic core plays a significant role in determining the overall stiffness of the sandwich plate.

3.2 Thermal post-buckling:

To ascertain the accuracy of the present formulation for postbuckling behaviour of plates, a validation study is conducted for a symmetrically laminated plate with stacking sequence $[0°/90°]_s$ with temperature-dependent properties. Material properties of the layers are highly dependent on temperature and are described according to the following expressions.

$$E_{11}(T) = 40 \times 10^9\left(1 - 0.5 \times 10^{-3}(T - T_0)\right)Pa,$$

$$E_{22}(T) = 1 \times 10^9\left(1 - 0.2 \times 10^{-3}(T - T_0)\right)Pa$$

$$G_{12}(T) = 0.5 \times 10^9\left(1 - 0.2 \times 10^{-3}(T - T_0)\right)Pa,$$

$$G_{13}(T) = 0.5 \times 10^9\left(1 - 0.2 \times 10^{-3}(T - T_0)\right)Pa$$

$$G_{23}(T) = 0.2 \times 10^9\left(1 - 0.2 \times 10^{-3}(T - T_0)\right)\text{Pa},$$

$$\alpha_{11}(\text{T}) = 1 \times 10^{-6}\left(1 + 0.5 \times 10^{-3}(\text{T} - \text{T}_0)\right)1/\text{K}$$

$$\alpha_{22}(\text{T}) = 10 \times 10^{-6}\left(1 + 0.5 \times 10^{-3}(\text{T} - \text{T}_0)\right)1/\text{K}$$

$$\text{v}_{12} = 0.25$$

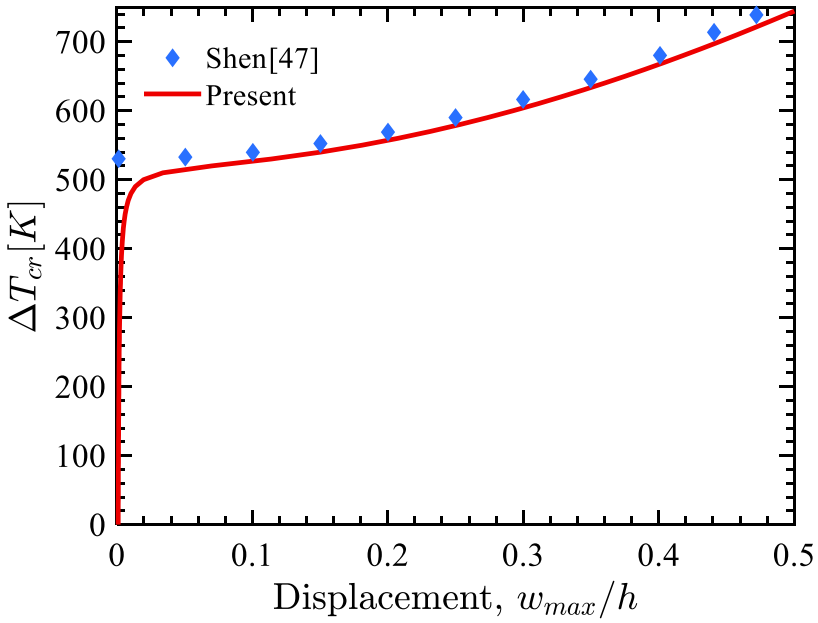


Fig. 3.Validation study for thermal postbuckling behaviour of laminated $[0°/90°]_s$ plate with temperature dependent properties subjected to uniform temperature rise (a/b = 1,a/h = 30)

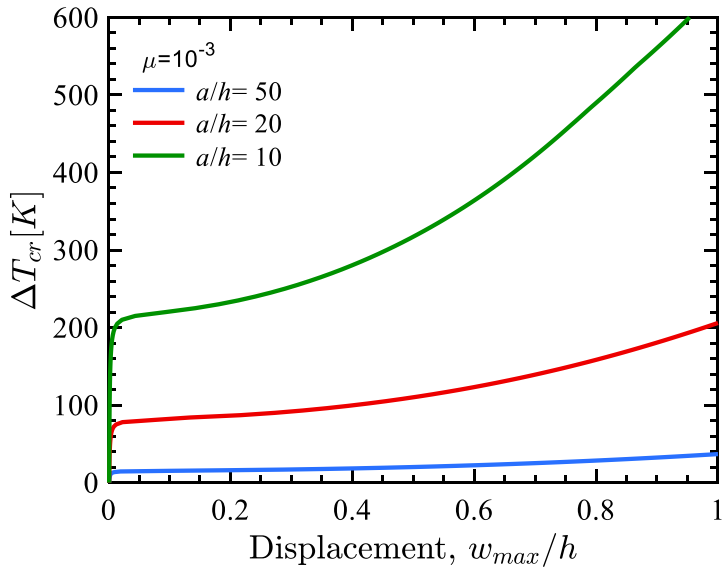


Fig. 4. Influence of width-to-plate thickness ratio of a sandwich plate on post-buckling behaviour subjected to uniform temperature rise($\frac{a}{h} = 100, \frac{h_2}{h} = 0.5, \frac{t}{l_1} = 0.1, \frac{l_1}{l_2} = 2, V^*_{CNT} 0.17, \theta_{hc}$=30°, UD, SSSS)

Fig. 3 includes the comparison of thermal post-buckling equilibrium path of a simply supported (SSSS) laminated $[0°/90°]_s$ plate (a/b=1, a/h = 30) plates with those given by Shen [47] obtained using a two-step perturbation technique. It is observed that the results are in close agreement, which confirms the accuracy of the present formulation. Fig. 4. presents the thermal post-buckling behaviour of plates with different a/h ratios. It is shown that the critical buckling temperature of sandwich plates increases as the a/h ratio decreases because with the increase in the thickness, the flexural rigidity of the plate increases.

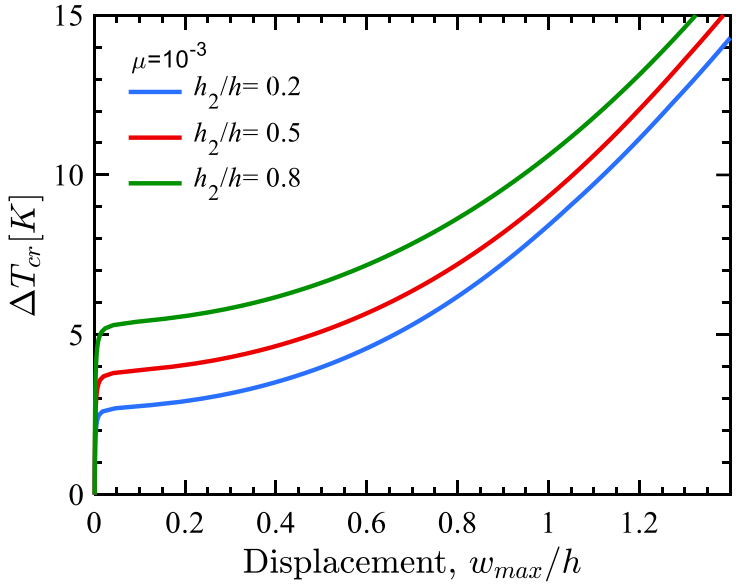


Fig. 5. Influence of core to a plate thickness of a square sandwich plate on post-buckling behaviour subjected to uniform temperate rise ($\frac{a}{h} = 100, \frac{h_2}{h} = 0.5$, $V^*_{CNT} = 0.17$, θ_{hc}=30°, $\frac{t}{l_1} = 0.1, \frac{l_1}{l_2} = 2$, UD, SSSS)

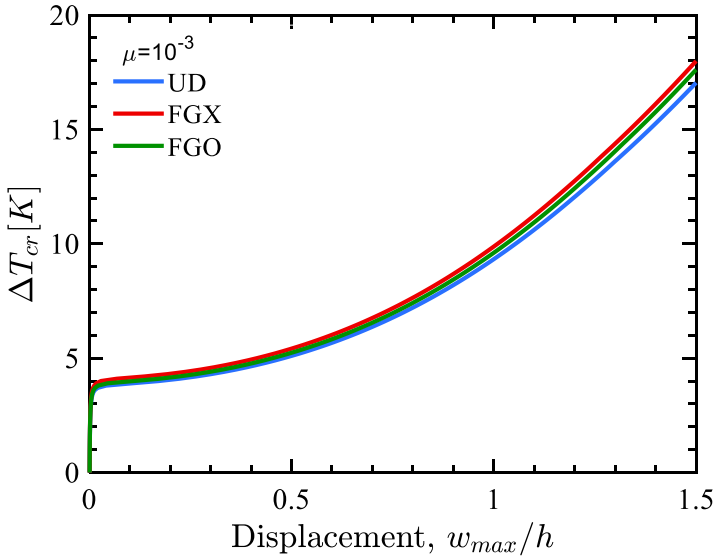


Fig. 6. Influence of CNT distribution in the face sheets of a square sandwich plate on post-buckling behaviour subjected to uniform temperature rise ($\frac{a}{h} = 100, \frac{h_2}{h} = 0.5, \frac{t}{l_1} = 0.1, \frac{l_1}{l_2} = 2$, θ_{hc}= 30°, $V^*_{CNT} = 0.17$, UD, SSSS)

Fig. 5 indicates the effect of core to plate thickness ratio on the square sandwich plate's thermal post-buckling equilibrium path with SSSS boundary conditions. The CNTs are assumed to be uniformly distributed in the face sheets. It is observed from the results that the critical buckling temperature of the sandwich plate may be enhanced by increasing the core-to-thickness ratio where the total thickness of the plate is constant. Fig. 6 shows the influence of CNT distribution in the face sheets of a square sandwich plate on post-buckling behaviour subjected to uniform temperature rise. The results indicate that the distribution of CNTs in the face sheets had very little effect on the thermal post-buckling equilibrium paths of sandwich plates with UD, FG-X, and FG-O distribution in face sheets.

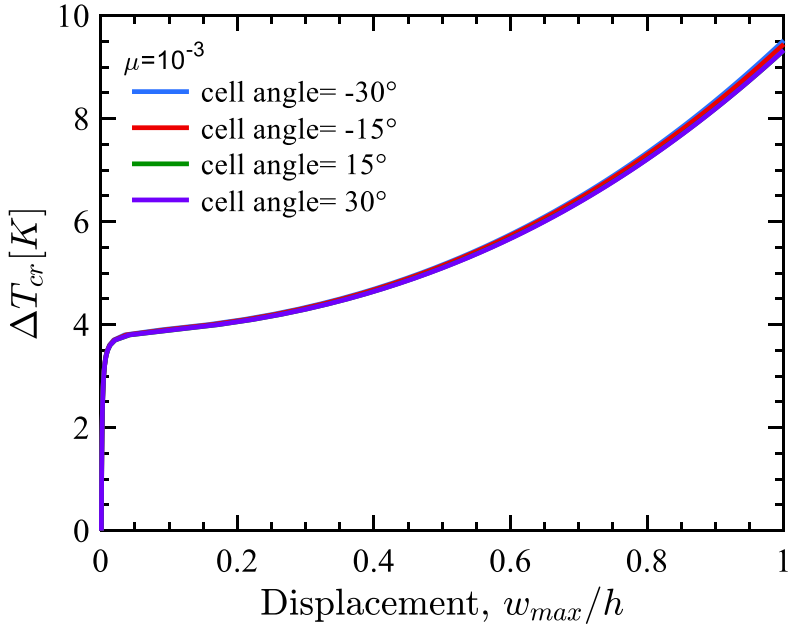


Fig. 7. Influence of core auxecity on a square andwich plate consists of isotropic face sheets on post-buckling behaviour subjected to uniform temperature rise (UD, $V^{*}_{CNT} = 0.17$, θ_{hc}=30°, $\frac{l_1}{l_2} = 2\,\frac{t}{l_1} = 0.1$, SSSS)

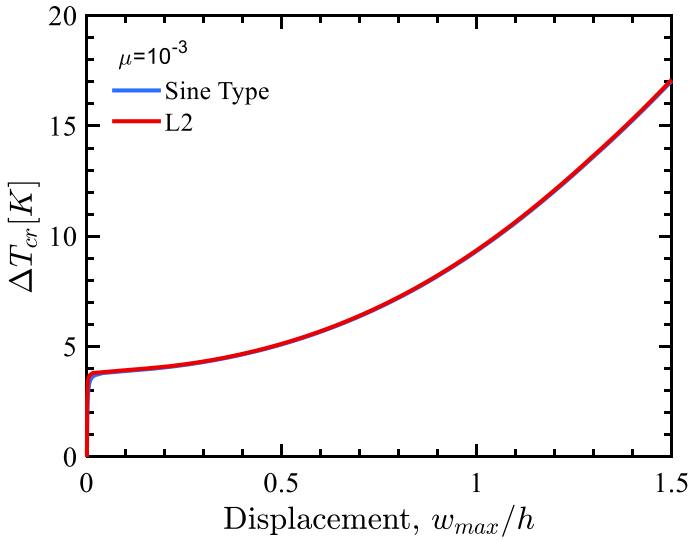


Fig. 8. Influence of types of imperfections of a sandwich plate on post-buckling behaviour subjected to uniform temperature rise($\frac{a}{h} = 100, \frac{h_2}{h} = 0.5, \frac{t}{l_1} = 0.1, \frac{l_1}{l_2} = 2, V^{*}_{CNT} = 0.17, \theta_{hc}$= 30°, UD,SSSS)

The cell angle in auxetic core geometry is a critical parameter influencing their unique mechanical properties and behaviour. In Fig.7, the thermal post-buckling equilibrium paths of sandwich plates with auxetic core for four different cell angles are considered. It is apparent from the results that the cell angle in the core geometry does not contribute towards the buckling strength of the structure. The sinusoidal and L_2-type imperfections on a plate can have significant post-buckling effects, influencing how the plate behaves after it has experienced buckling. Fig. 8 shows the post-buckling behaviour of a square sandwich plate under the two different types of initial imperfections, i.e., sine type and L_2 type. It is observed from the figure that thermal post-buckling equilibrium paths of sandwich plates with sine type and L_2 type imperfections are similar due to the similar shape of imperfections.

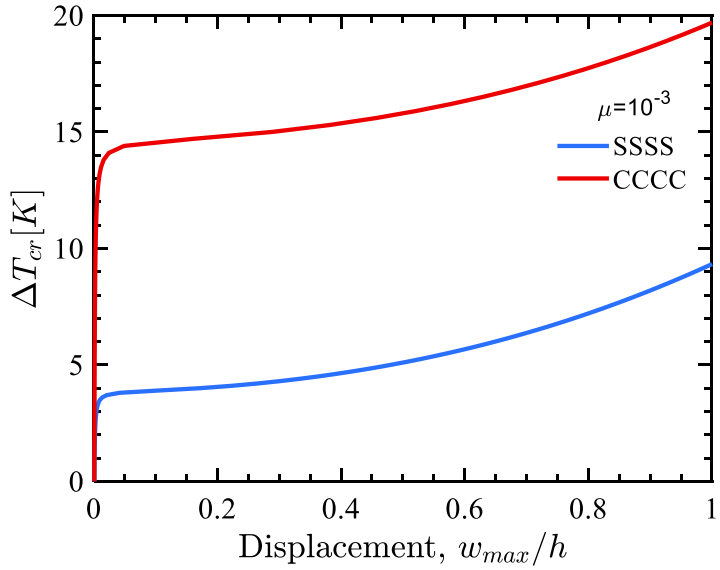


Fig. 9. Influence of boundary conditions of the square sandwich plate on post-buckling behaviour subjected to thermal load ($\frac{a}{h} = 100, \frac{h_2}{h} = 0.5$, $V^*_{CNT} = 0.17$, θ_{hc}=30°, $\frac{t}{l_1} = 0.1$, $\frac{l_1}{l_2} = 2$, UD)

The effect of boundary conditions on the square sandwich plate, including an auxetic core, is shown in Fig. 9. As expected, CCCC plates' critical buckling temperature is higher than SSSS plates'. This observed trend may be ascribed to an edge clamped being stiffer than an edge just simply supported.

4 Conclusions:

The linear and nonlinear thermal postbuckling behaviour of sandwich plate with FGCNTRC face sheets and an auxetic core is investigated using isogeometric approach. The mathematical formulation is based on a refined higher order theory with nonlinear strain displacement relations with von Karman assumptions. The nonlinear algebraic equations are solved using Newton-Raphson method. Validation studies indicate that the results obtained using the present formulation are in very good agreement with those available in the literature. New results on the influence of CNT distribution in the facesheets, viz., UD, FGX, FGO, core auxeticity, span to thickness ratio, core to plate thickness ratio, different shapes of initial imperfection and boundary conditions on thermal buckling temperature, hitherto not found in the literature are presented for the first time. It is observed that with the increase in the volume fraction of CNTs, the critical buckling temperature of the plate increases. The critical buckling temperature of sandwich plates may also be enhanced by increasing the core-to-plate thickness ratio. Moreover, initial geometric imperfections may significantly influence the post-buckling responses of the sandwich plate.

Conflicts of Interest Statement: The corresponding author declares no conflict of interest on behalf of all authors.

Acknowledgments

The authors acknowledge the support provided by BITS Pilani, Pilani Campus, Sanjivani University, Kopargaon and Gramya Innovative Technologies, Greater Noida.

Disclosure statement

No potential conflict of interest was reported by the author(s).

Funding

No Funding

5 References:

[1] R. Lakes, "Foam Structures with a Negative Poisson's Ratio," Science (80-.)., vol. 235, no. 4792, pp. 1038–1040, 1987, doi: 10.1126/science.235.4792.1038.

[2] K. L. Alderson and K. E. Evans, "Auxetic materials: the positive side of being negative," Eng. Sci. Educ. J., vol. 9, no. 4, pp. 148–154, 2000, doi: 10.1049/esej:20000402.

[3] K. E. Evans, M. A. Nkansah, and I. J. Hutchinson, "Auxetic foams: Modelling negative Poisson's ratios," Acta Metall. Mater., vol. 42, no. 4, pp. 1289–1294, 1994, doi: 10.1016/0956-7151(94)90145-7.

[4] D. De Rossi, Biomimetic materials and structures, vol. 2779. 1996. doi: 10.1117/12.237109.

[5] A. Alderson and K. L. Alderson, "Auxetic materials," Proc. Inst. Mech. Eng. Part G J. Aerosp. Eng., vol. 221, no. 4, pp. 565–575, 2007, doi: 10.1243/09544100JAERO185.

[6] M. Mir, M. N. Ali, J. Sami, and U. Ansari, "Review of mechanics and applications of auxetic structures," Adv. Mater. Sci. Eng., vol. 2014, pp. 1–18, 2014, doi: 10.1155/2014/753496.

[7] K. R. Thangaratnam, Palaninathan, and J. Ramachandran, "Thermal buckling of composite laminated plates," Comput. Struct., vol. 32, no. 5, pp. 1117–1124, 1989, doi: 10.1016/0045-7949(89)90413-6.

[8] K. S. Na and J. H. Kim, "Thermal postbuckling investigations of functionally graded plates using 3-D finite element method," Finite Elem. Anal. Des., vol. 42, no. 8–9, pp. 749–756, 2006, doi: 10.1016/j.finel.2005.11.005.

[9] S. Trabelsi, A. Frikha, S. Zghal, and F. Dammak, "Thermal post-buckling analysis of functionally graded material structures using a modified FSDT," Int. J. Mech. Sci., vol. 144, pp. 74–89, 2018, doi: 10.1016/j.ijmecsci.2018.05.033.

[10] K. Mehar, S. Kumar Panda, Y. Devarajan, and G. Choubey, "Numerical buckling analysis of graded CNT-reinforced composite sandwich shell structure under thermal loading," Compos. Struct., vol. 216, pp. 406–414, 2019, doi: 10.1016/j.compstruct.2019.03.002.

[11] E. Harkati, N. Daoudi, A. Bezazi, A. Haddad, and F. Scarpa, "In-plane elasticity of a multi re-entrant auxetic honeycomb," Compos. Struct., vol. 180, pp. 130–139, 2017, doi: 10.1016/j.compstruct.2017.08.014.

[12] M. M. Alipour and M. Shariyat, Analytical layerwise free vibration analysis of circular/annular composite sandwich plates with auxetic cores, Int J Mech Mater Des, vol. 13, no. 1, 2017. doi: 10.1007/s10999-015-9321-2.

[13] M. Sarafraz, H. Seidi, F. Kakavand, and N. S. Viliani, "Free vibration and buckling analyses of a rectangular sandwich plate with an auxetic honeycomb core and laminated three-phase polymer/GNP/fiber face sheets," Thin-Walled Struct., vol. 183, no. 2022, p. 110331, 2023, doi: 10.1016/j.tws.2022.110331.

[14] C. Li, H. S. Shen, and H. Wang, "Postbuckling behavior of sandwich plates with functionally graded auxetic 3D lattice core," Compos. Struct., vol. 237, p. 111894, 2020, doi: 10.1016/j.compstruct.2020.111894.

[15] X. Chen, H. S. Shen, and X. H. Huang, "Thermo-mechanical postbuckling analysis of sandwich plates with functionally graded auxetic GRMMC core on elastic foundations," Compos. Struct., vol. 279, p. 114796, 2022, doi: 10.1016/j.compstruct.2021.114796.

[16] V. D. Quang, T. Q. Quan, and P. Tran, "Static buckling analysis and geometrical optimization of magneto-electro-elastic sandwich plate with auxetic honeycomb core," Thin-Walled Struct., vol. 173, p. 108935, 2022, doi: 10.1016/j.tws.2022.108935.

[17] J. Torabi, R. Ansari, and R. Hassani, "Numerical study on the thermal buckling analysis of CNT-reinforced composite plates with different shapes based on the higher-order shear deformation theory," Eur. J. Mech. A/Solids, vol. 73, no. 2018, pp. 144–160, 2019, doi: 10.1016/j.euromechsol.2018.07.009.

[18] T. Kant and C. S. Babu, "Thermal buckling analysis of skew fibre-reinforced composite and sandwich plates using shear deformable finite element models," vol. 49, pp. 77–85, 2000.

[19] M. K. Singha, L. S. Ramachandra, and J. N. Bandyopadhyay, "Thermal postbuckling analysis of laminated composite plates," vol. 54, pp. 453–458, 2001.

[20] T. Prakash, M. K. Singha, and M. Ganapathi, "Thermal postbuckling analysis of FGM skew plates," Eng. Struct., vol. 30, no. 1, pp. 22–32, 2008, doi: 10.1016/j.engstruct.2007.02.012.

[21] G. Watts, R. Kumar, S. Singh, V. Sengar, G. R. Reddy, and S. N. Patel, "Postbuckling and postbuckled vibration behaviour of imperfect trapezoidal sandwich plates with FG-CNTRC face sheets under nonuniform loadings," Aerosp. Sci. Technol., vol. 127, p. 107716, 2022, doi: 10.1016/j.ast.2022.107716.

[22] T. J. R. Hughes, J. A. Cottrell, and Y. Bazilevs, "Isogeometric analysis: CAD, finite elements, NURBS, exact geometry and mesh refinement," Comput. Methods Appl. Mech. Eng., vol. 194, no. 39–41, pp. 4135–4195, 2005, doi: 10.1016/j.cma.2004.10.008.

[23] W. Fang, J. Zhang, T. Yu, and T. Q. Bui, "Analysis of thermal effect on buckling of imperfect FG composite plates by adaptive

XIGA," Compos. Struct., vol. 275, no, p. 114450, 2021, doi: 10.1016/j.compstruct.2021.114450.

[24] M. Mirzaei and Y. Kiani, "Isogeometric thermal buckling analysis of temperature dependent FG graphene reinforced laminated plates using NURBS formulation," Compos. Struct., vol. 180, pp. 606–616, 2017, doi: 10.1016/j.compstruct.2017.08.057.

[25] H. Mohammadi, "Isogeometric thermal buckling analysis of GPL reinforced composite laminated folded plates," Eng. Struct., vol. 255, no. January, p. 113905, 2022, doi: 10.1016/j.engstruct.2022.113905.

[26] V. N. Van Do and C. H. Lee, "Quasi-3D isogeometric buckling analysis method for advanced composite plates in thermal environments," Aerosp. Sci. Technol., vol. 92, pp. 34–54, 2019, doi: 10.1016/j.ast.2019.05.056.

[27] H. Nguyen-Xuan, L. V. Tran, C. H. Thai, S. Kulasegaram, and S. P. A. Bordas, "Isogeometric analysis of functionally graded plates using a refined plate theory," Compos. Part B Eng., vol. 64, pp. 222–234, 2014, doi: 10.1016/j.compositesb.2014.04.001.

[28] V. Nguyen Van Do and C. H. Lee, "Isogeometric analysis for buckling and postbuckling of graphene platelet reinforced composite plates in thermal environments," Eng. Struct., vol. 244, p. 112746, 2021, doi: 10.1016/j.engstruct.2021.112746.

[29] L. V. Tran, P. Phung-Van, J. Lee, M. A. Wahab, and H. Nguyen-Xuan, "Isogeometric analysis for nonlinear thermomechanical stability of functionally graded plates," Compos. Struct., vol. 140, pp. 655–667, 2016, doi: 10.1016/j.compstruct.2016.01.001.

[30] Y. Kiani, "NURBS-based thermal buckling analysis of graphene platelet reinforced composite laminated skew plates," J. Therm. Stress., vol. 43, no. 1, pp. 90–108, 2020, doi: 10.1080/01495739.2019.1673687.

[31] Y. Kiani, "NURBS-based isogeometric thermal postbuckling analysis of temperature dependent graphene reinforced composite laminated plates," Thin-Walled Struct., vol. 125, pp. 211–219.

[32] V. Sengar, M. Nynaru, G. Watts, R. Kumar, and S. Singh, "Postbuckled vibration behaviour of skew sandwich plates with metal foam core under arbitrary edge compressive loads using isogeometric approach," Thin-Walled Struct., vol. 184, p. 110524, 2023, doi: 10.1016/j.tws.2023.110524.

[33] A. Farzam and B. Hassani, "Thermal and mechanical buckling analysis of FG carbon nanotube reinforced composite plates using modified couple stress theory and isogeometric approach," Compos. Struct., vol. 206, pp. 774–790, 2018, doi: 10.1016/j.compstruct.2018.08.030.

[34] L. W. Zhang, M. Memar Ardestani, and K. M. Liew, "Isogeometric approach for buckling analysis of CNT-reinforced composite skew plates under optimal CNT-orientation," Compos. Struct., vol. 163, pp. 365–384.

[35] N. Valizadeh, T. Q. Bui, V. T. Vu, H. T. Thai, and M. N. Nguyen, "Isogeometric simulation for buckling, free and forced vibration of orthotropic plates," Int. J. Appl. Mech., vol. 5, no. 2, 2013, doi: 10.1142/S1758825113500178.

[36] T. Le-Manh and J. Lee, "Postbuckling of laminated composite plates using NURBS-based isogeometric analysis," Compos. Struct., vol. 109, no. 1, pp. 286–293, 2014, doi: 10.1016/j.compstruct.2013.11.011.

[37] Y. Kiani, "Thermal post-buckling of temperature dependent sandwich plates with FG-CNTRC face sheets," J. Therm. Stress., vol. 41, no. 7, pp. 866–882, 2018, doi: 10.1080/01495739.2018.1425645.

[38] Q. Jiang, S. S. Tallury, Y. Qiu, and M. A. Pasquinelli, "Molecular dynamics simulations of the effect of the volume fraction on unidirectional polyimide-carbon nanotube nanocomposites," Carbon, vol. 67, pp. 440–448, 2014, doi: 10.1016/j.carbon.2013.10.016.

[39] Z. X. Wang and H. S. Shen, "Nonlinear vibration and bending of sandwich plates with nanotube-reinforced composite face sheets," Compos. Part B Eng., vol. 43, no. 2, pp. 411–421, Mar. 2012.

[40] A. Gupta and S. Pradyumna, "Nonlinear dynamic analysis of sandwich shell panels with auxetic honeycomb core and curvilinear fibre reinforced facesheets," Eur. J. Mech. A/Solids, vol. 95, p. 104640, 2022, doi: 10.1016/j.euromechsol.2022.104640.

[41] G. Watts, S. Singh, and F. Pathan, "Meshfree analysis of non-rectangular sandwich plates based on refined C0 higher order shear deformation theories," Eng. Anal. Bound. Elem., vol. 120, pp. 180–194, 2020, doi: 10.1016/j.enganabound.2020.08.011.

[42] S. Kitipornchai, J. Yang, and K. M. Liew, "Semi-analytical solution for nonlinear vibration of laminated FGM plates with geometric imperfections," Int. J. Solids Struct., vol. 41, no. 9–10, pp. 2235–2257, 2004, doi: 10.1016/j.ijsolstr.2003.12.019.

[43] S. Trabelsi, S. Zghal, and F. Dammak, "Thermo-elastic buckling and post-buckling analysis of functionally graded thin plate and shell structures," J. Brazilian Soc. Mech. Sci. Eng., vol. 42, no. 5, pp. 1–22, 2020, doi: 10.1007/s40430-020-02314-5.

[44] H. S. Shen and C. L. Zhang, "Thermal buckling and postbuckling behavior of functionally graded carbon nanotube-reinforced composite plates," Mater. Des., vol. 31, no. 7, pp. 3403–3411, 2010, doi: 10.1016/j.matdes.2010.01.048.

[45] Y. Kiani, "Thermal buckling of temperature-dependent FG-CNT-reinforced composite skew plates," J. Therm. Stress., vol. 40, no. 11, pp. 1442–1460, doi: 10.1080/01495739.2017.1336742.

[46] M. Cetkovic, "Influence of initial geometrical imperfections on thermal stability of laminated composite plates using layerwise finite element," Compos. Struct., vol. 291, p. 115547, 2022, doi: 10.1016/j.compstruct.2022.115547.

[47] H. S. Shen, "Thermal postbuckling behavior of imperfect shear deformable laminated plates with temperature-dependent properties," Comput. Methods Appl. Mech. Eng., vol. 190, pp. 5377–5390, Jul. 2001, doi: 10.1016/S0045-7825(01)00172-4.

479

480

481

482